Learning effective physical laws for generating cosmological hydrodynamics with Lagrangian deep learning

Biwei Dai (戴必玮)[a,b,1] and Uroš Seljak[a,b,c,d]

[a]Berkeley Center for Cosmological Physics, University of California, Berkeley, CA 94720; [b]Department of Physics, University of California, Berkeley, CA 94720; [c]Department of Astronomy, University of California, Berkeley, CA 94720; and [d]Physics Division, Lawrence Berkeley National Laboratory, Berkeley, CA 94720

Edited by Neta A. Bahcall, Princeton University, Princeton, NJ, and approved March 1, 2021 (received for review October 8, 2020)

The goal of generative models is to learn the intricate relations between the data to create new simulated data, but current approaches fail in very high dimensions. When the true data-generating process is based on physical processes, these impose symmetries and constraints, and the generative model can be created by learning an effective description of the underlying physics, which enables scaling of the generative model to very high dimensions. In this work, we propose Lagrangian deep learning (LDL) for this purpose, applying it to learn outputs of cosmological hydrodynamical simulations. The model uses layers of Lagrangian displacements of particles describing the observables to learn the effective physical laws. The displacements are modeled as the gradient of an effective potential, which explicitly satisfies the translational and rotational invariance. The total number of learned parameters is only of order 10, and they can be viewed as effective theory parameters. We combine N-body solver fast particle mesh (FastPM) with LDL and apply it to a wide range of cosmological outputs, from the dark matter to the stellar maps, gas density, and temperature. The computational cost of LDL is nearly four orders of magnitude lower than that of the full hydrodynamical simulations, yet it outperforms them at the same resolution. We achieve this with only of order 10 layers from the initial conditions to the final output, in contrast to typical cosmological simulations with thousands of time steps. This opens up the possibility of analyzing cosmological observations entirely within this framework, without the need for large dark-matter simulations.

deep learning | Lagrangian approach | cosmological hydrodynamical simulation

Numerical simulations of large-scale structure formation in the universe are essential for extracting cosmological information from the observations (1–7). In principle, hydrodynamical simulations are capable of predicting the distribution of all observables in the universe and thus can model observations directly. However, running high-resolution hydrodynamical simulations at volumes comparable to those of the current and future sky surveys is currently not feasible, due to its high computational costs. The most widely used method is running gravity-only N-body simulations and then populating baryons in the halo catalogs with semianalytical approaches such as halo occupation distribution (HOD) (8) or halo assembly models (9). However, these methods make strong assumptions such as the halo mass being the main quantity controlling the baryonic properties. In addition, many of the cosmological observations such as X-ray emission and Sunyaev–Zeldovich (SZ) emission are based on hydrodynamic gas properties such as gas density, temperature, pressure, etc., which cannot be modeled in the dark matter-only simulations.

Deep-learning methods provide an alternative way to model the cosmological observables. A number of papers view the task as an image-to-image translation problem; i.e., they take in pixelized matter density field as input data and output the target pixelized observable field. These methods either model the conditional probability distribution $p(y_{target}|x_{input})$ using deep generative models such as generative adversarial networks (GANs) (10) and variational autoencoders (VAEs) (11, 12) or learn a mapping $x_{input} \mapsto y_{target}$ with deep convolutional neural networks (DCNNs). Previous work in this area covers a wide array of tasks, such as identifying halos (protohalos) (13–16), producing three-dimensional (3D) galaxy distribution (17), generating thermal SZ (tSZ) signals (18), predicting dark matter annihilation feedback (19), learning neutrino effects (20), and emulating high-resolution features from low-resolution simulations (21, 22), etc.

Unlike these methods that work in pixel (Eulerian) space and treat the field as images, another way to model the dynamics is to adopt the Lagrangian scheme, i.e., trace the motion of individual particles or fluid elements by modeling their displacement field. The displacement field contains more information than the density field, as different displacement fields can produce the same density field, and is in general more Gaussian and linear than the density field. Existing methods in this space cover only the dark matter, e.g., approximate N-body solvers (23, 24) and DCNNs (25).

In this work we propose a deep-learning architecture, Lagrangian deep learning (LDL), for modeling both the cosmological dark matter and the hydrodynamics, using the Lagrangian approach. The model is motivated by the effective theory ideas in physics, where one describes the true process, which may be too complicated to model, with an effective, often coarse-grained,

Significance

Hydrodynamical simulations are crucial for accurately predicting cosmological observations, but they are computationally too expensive to simulate in a full survey volume. Gravity-only N-body simulations reduce the computational cost but cannot directly model the observables such as stars and gas. Here we propose a deep-learning approach to generate these observables. The model consists of several layers of Lagrangian displacement field moving the particles. It requires only a handful of parameters to learn, in contrast to neural networks, and can be viewed as learning the effective physical laws. By combining N-body solvers with our model, we are able to generate higher-accuracy hydrodynamic observables with computational costs several orders of magnitude cheaper than the traditional hydrodynamical simulations at the same resolution.

Author contributions: B.D. and U.S. designed research; B.D. performed research; B.D. analyzed data; and B.D. and U.S. wrote the paper.

The authors declare no competing interest.

This article is a PNAS Direct Submission.

[1]To whom correspondence may be addressed. Email: biwei@berkeley.edu.

Published April 14, 2021.

description of physics. A typical example is the effective field theory, where perturbative field theory is supplemented with effective field theory terms that obey the symmetries and are an effective coarse-grained description of the nonperturbative small-scale effects. The resulting effective description has a similar structure to that of the true physics, but with free coefficients that one must fit for, and that account for the nonperturbative small-scale effects.

Lagrangian Deep Learning

A cosmological dark matter and baryon evolution can be described by a system of partial differential equations (PDEs) coupling gravity, hydrodynamics, and various subgrid physics modeling processes such as the star formation, which are evolved in time from the beginning of the universe until today. One would wish to simulate a significant fraction of the observable universe, while also capturing important physical processes on orders of magnitude smaller scales, all in three dimensions. As a result, the resulting dynamical range is excessive even for the modern computational platforms. As an example, the state-of-the-art The Next Generation Illustris project TNG300-1 (26–30) has of order 10^{10} particles, yet simulates only a very small fraction of observable universe. The lower-resolution TNG300-3 reduces the number of particles by 64, at a cost of significantly reducing the realism of the simulation.

An effective physics approach is to rewrite the full problem into a large-scale problem that we can solve, together with an effective description of the small scales which we cannot resolve. In theoretical physics this is typically done by rewriting the Lagrangian such that it takes the most general form that satisfies the symmetries of the problem, with free coefficients describing the effect of the small-scale coarse graining. In cosmology the large-scale evolution is governed by gravity, which can easily be solved perturbatively or numerically. Effective descriptions using perturbative expansions exist (31), but fail to model small scales and complicated baryonic processes at the map level. While spatial coarse graining is the most popular implementation of this idea, one can also apply it to temporal coarse graining. A typical PDE solver requires many time steps, which is expensive. Temporal coarse graining replaces this with fewer integration time steps, at a price of replacing the true physics equations with their effective description, while ensuring the true solution on large scales, where the solution is known (23, 24).

Here we take this effective physics description idea and combine it with the deep-learning paradigm, where one maps the data through several layers consisting of simple operations and trains the coefficients of these layers on some loss function of choice. While machine-learning layers are described with neural networks with a very large number of coefficients, here we will view a single layer as a single time-step PDE solver, using a similar structure to that of the true physical laws.* This has the advantage that it can preserve the symmetries inherent in the problem. The main symmetry we wish to preserve in a cosmological setting is the translational and rotational symmetry: The physical laws have no preferred position or direction. But we also wish to satisfy the existing conservation laws, such as the dark matter and baryon mass conservation.

A very simple implementation of these two requirements is Lagrangian displacements of particles describing the dark matter or baryons. We displace the particles using the gradient of a potential, and mass conservation is ensured since we only move the particles around. To ensure the translation and rotation symmetry within the effective description we shape the potential in Fourier space, such that it depends only on the amplitude of the Fourier wave vector. The potential gradient can be viewed as a force acting upon their acceleration via Newton's law, and the shaping of the potential is equivalent to the radial dependence of the force. This description requires particle positions and velocities, so it is a second-order PDE in time. We will use this description for the dark matter. However, for baryons we can simplify the modeling by assuming their velocity is the same as that of the dark matter, since velocity is dominated by large scales where the two trace each other. In this case we can use the potential gradient to displace particle positions directly, so the description becomes effectively first order in time. Moreover, by a simple extension of the model we can apply this concept to the baryonic observables such as the gas pressure and temperature, where conservation laws no longer apply. A complete description also requires us to define the source for the potential. In physics this is typically some property of the particles, such as mass or charge. Here we wish to describe the complicated nonlinear processes of subgrid physics, as well as coarse graining in space and time. Motivated by gravity we will make the simplest possible assumption of the source being a simple power law of the density, using a learned Green's function to convert to the potential. Since we wish to model several different physics processes, we stack it into multiple layers. Because the model takes in the particle data and models the displacement field from the Lagrangian approach using multiple layers, we call this model LDL.

Our specific goal is to model the distribution of dark matter and hydrodynamic observables starting from the initial conditions as set in the early universe, using an effective description that captures the physics symmetries and conservation laws. An example of such a process applied to time and spatial coarse graining is the dark matter evolution with a few time steps only, which combines ideas such as the approximate N-body solvers, with a force sharpening process called potential gradient descent (PGD) to capture the coarse graining (32, 33). We first use FastPM (24), a quasi–particle-mesh (PM) N-body solver, which ensures the correct large-scale growth at any number of time steps, since the kick and drift factors of the leapfrog integrator in FastPM are modified following the linear (Zel'dovich) equation of motion. FastPM has a few layers only (typically 5 to 10) and uses particle displacements. It is supplemented by one additional layer of PGD applied to position only to improve the dark matter distribution on small scales. All of the steps of this process are in the LDL form, so can be viewed as its initial layers. The resulting dark matter maps are shown in Fig. 1 and show an excellent agreement with the full N-body simulation of Illustris TNG, which is also confirmed by numerical comparisons presented in ref. 32. This application is not learning new physics, but is learning the effective physics description of both time and spatial coarse graining: Instead of 1,000+ time steps in a standard N-body simulation we use only 10, and instead of the full spatial resolution we will use a factor of 64 reduced mass resolution.

Here we wish to extend these ideas to the more complex and expensive problem of cosmological hydrodynamics, where we wish to learn its physics using an effective description. Baryons are dissipative and collisional, with many physical processes, such as cooling, radiation, star formation, gas shocks, turbulence, etc., happening inside the highest-density regions called dark matter halos. One can add displacements to the dark matter particles to simulate these hydrodynamic processes, such that the particles after the displacement have a similar distribution to that of the baryons. Enthalpy gradient descent (EGD) is an example of this idea (32): One adds small-scale displacement to the dark matter particles to improve the small scales of the low-resolution

*In the rest of this paper we will refer to each step of the model as one layer, to emphasize the fact that our model is parameterized by free parameters that need to be trained on hydrosimulations. However, one should note that in this research we do not use any actual neural networks. Since the FastPM time step can be viewed as a special case of our model, we will also refer to each FastPM time step as one layer, even though the parameters (e.g., kick and drift factors) are determined by physics rather than fitting to some loss functions.

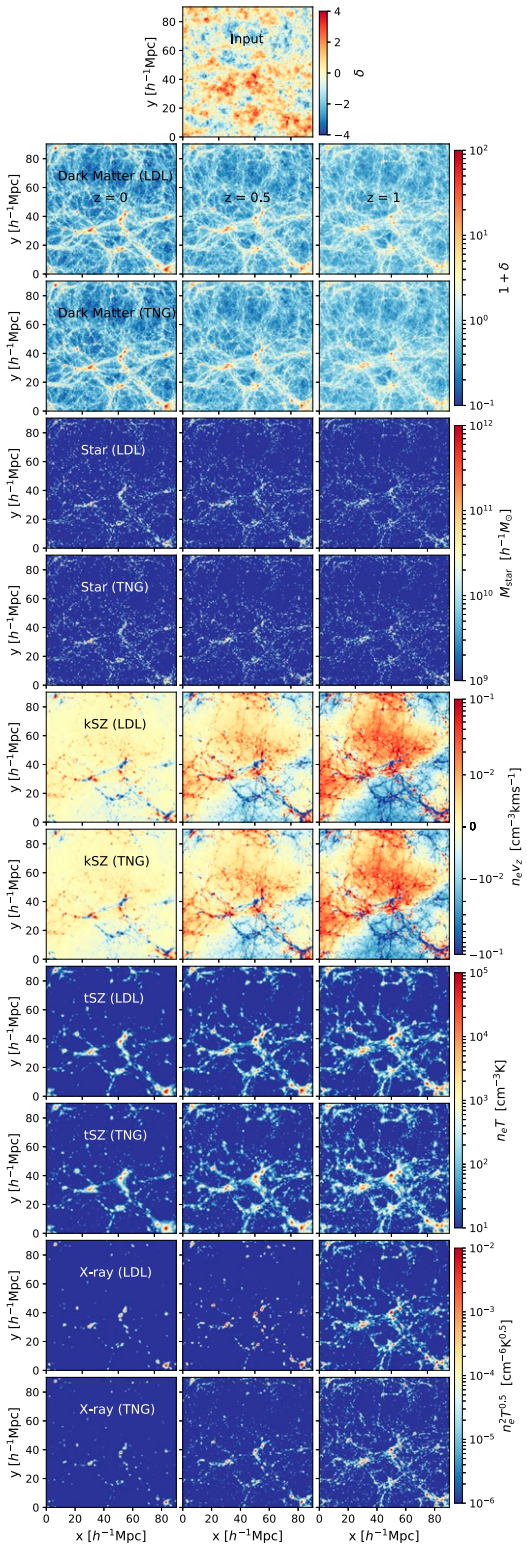

Fig. 1. Visualization of slices of the simulations. The first row is the input linear density field. The 2nd, 4th, 6th, 8th, and 10th rows are predictions of dark matter overdensity, stellar mass, electron momentum density $n_e v_z$ (kSZ signal), electron pressure $n_e T$ (tSZ signal), and $n_e^2 T^{0.5}$ (X-ray signal) from our FastPM + LDL hybrid simulation, respectively. The 3rd, 5th, 7th, 9th, and 11th rows are the corresponding target fields from TNG300-1 hydrodynamical simulation. *Left*, *Center*, and *Right* columns are from redshift $z = 0$, $z = 0.5$, and $z = 1$, respectively. The slices are from a $90.2 \times 90.2 \times 32.8$ h^{-1}Mpc subbox of the test set.

approximate simulations and to model the baryonic feedback on the total matter distribution. Motivated by these methods, we propose to model this displacement field by

$$\mathbf{S} = \alpha \nabla \hat{\mathbf{O}}_{\mathbf{G}} f(\delta), \qquad [1]$$

where α is a learnable parameter, δ is the matter overdensity as output by the initial layers (FastPM and LDL on dark matter layer), and $f(\delta)$ is the source term and can be an arbitrary function of δ. Here we choose it to be a power law

$$f(\delta) = (1+\delta)^{\gamma}, \qquad [2]$$

with γ a learnable parameter. $\hat{\mathbf{O}}_{\mathbf{G}}$ is Green's operator and can be written explicitly as

$$\hat{\mathbf{O}}_{\mathbf{G}} f(\delta) = \int G(\mathbf{x}-\mathbf{x}') f(\delta(\mathbf{x}'))\, d\mathbf{x}', \qquad [3]$$

where $G(\mathbf{x}-\mathbf{x}')$ is the Green's function and we have used $G(\mathbf{x},\mathbf{x}') = G(\mathbf{x}-\mathbf{x}')$ due to translational symmetry. The convolution in the above equation can be easily calculated in Fourier space as $\hat{\mathbf{O}}_{\mathbf{G}} f(\delta) = G(\mathbf{k}) f(\delta)$, and we further have $G(\mathbf{k}) = G(k)$ because of the rotational symmetry of the system. Following the PGD model, we model $\hat{\mathbf{O}}_{\mathbf{G}}$ in Fourier space as

$$\hat{\mathbf{O}}_{\mathbf{G}} = \exp(-(k_h/k)^2)\exp(-(k/k_l)^2)\, k^n, \qquad [4]$$

where k_h, k_l, and n are additional learnable parameters. The high-pass filter $\exp(-(k_h/k)^2)$ prevents the large-scale growth, since the baryonic physics that we are trying to model are an effective description of the small-scale physics, while the large scales are correctly described by the linear perturbative solution enforced by FastPM. Together with the low-pass filter $\exp(-(k/k_l)^2)$, which has the typical effective theory form, the operator $\hat{\mathbf{O}}_{\mathbf{G}}$ is capable of learning the characteristic scale of the physics we are trying to model. Note that both the source $f(\delta)$ and the shape of $\hat{\mathbf{O}}_{\mathbf{G}}$ characterize the complex baryon and subgrid physics and cannot be derived from first principles. They can only be learned from high-resolution hydrodynamical simulations. As a special case, Eq. **1** can be used to represent the gravitational force if we set $\alpha = 4\pi G\bar{\rho}$, $\gamma = 1$, $k_h = 0$, $k_l = \infty$, and $n = -2$, but we allow all these parameters to vary to model the physics that are different from gravity. Eqs. **1**–**4** define the displacement field of one Lagrangian layer. We can stack multiple such layers to form a deep-learning model, where each layer takes the particle output from the previous layer (which determines δ in Eq. **1**) and adds additional displacements to the particles. Such a deep model will be able to learn more complex physics. The idea is that different layers can focus on different physics components, which will differ in terms of the scale dependence of the potential and its gradient, as well as in terms of the source density dependence.

We have made the assumption that the displacement field can be approximated by a sequence of irrotational vector fields, which are modeled by the gradient of some effective potential fields. This parameterization, although motivated by physics, is not derived from first principles and its effectiveness has to be examined by experiments. In principle, one could also use second-order equations for modeling the displacement fields, just like the true dynamics, at the cost of introducing one more free parameter per layer. Note that here we are trying only to effectively mimic the missing baryonic physics rather than actually simulating them, so the order of the equation does not matter. As we show in this paper, the first-order equation works

well enough for the resolution we considered, and thus we do not consider the second-order parameterizations.

The final output layer is modeled as a nonlinear transformation on the particle density field,

$$F(x) = \mathrm{ReLU}(b_1(1+\delta'(x))^{\mu} - b_0), \quad [5]$$

where F is the output target field; $\mathrm{ReLU}(x)$ is the rectified linear unit, which is zero if $x<0$ and x otherwise; δ' is the particle overdensity field after the displacement; and b_0, b_1, and μ are learnable parameters. This is motivated by the physics processes that cannot be modeled as a matter transport (i.e., displacement). In the example of stars, the Lagrangian displacement layers are designed to learn the effect of gas cooling and collapse. After these displacement layers, the particles are moved toward the halo center, where protogalaxies are formed and we expect star formation to happen in these dense regions. This star formation process is modeled by Eq. **5**: The ReLU thresholding aims at selecting the high-density regions where the star formation happens. Such thresholding is typical of a subgrid physics model: In the absence of this thresholding we would need to transport all of the particles out of the low-density regions where the star formation does not happen, a process that does not have a corresponding physical model.

The baryon process in the universe also leaves imprints on the total matter distribution (34–36). This feedback is crucial for accurately predicting the total matter distribution (e.g., in weak lensing applications). In this research, however, we mainly focus on modeling the distribution of baryon tracers and do not consider this feedback effect. We refer interested readers to the EGD model (32), which is a special case of LDL and has been shown to successfully model the baryonic feedback on the total matter distribution. We expect that LDL can also be applied to model this effect in a similar manner.

In this work we use both FastPM and N-body simulations, combining them with LDL to predict the baryon observables from the linear density map. We consider modeling the stellar mass, kinetic SZ (kSZ) signal, tSZ signal, and X-ray at redshift $z=1$, $z=0.5$, and $z=0$. The dark matter particles are first evolved to these redshifts with FastPM and then passed to the LDL networks for modeling the baryons. The parameters in LDL are optimized by matching the output with the target fields from TNG300-1 hydrodynamical simulation (26–30). Since the kSZ signal is proportional to the electron momentum $n_e v_z$, the tSZ signal is proportional to the electron pressure $n_e T$, and the X-ray emissivity is approximately proportional to $n_e^2 T^{0.5}$ (we consider only the bremsstrahlung effect and ignore the Gaunt factor), we will model these fields in the rest of this paper. See *Materials and Methods* for details on the FastPM/N-body + LDL hybrid simulations, as well as the training of the LDL parameters.

Apart from FastPM, we also consider combining LDL models with full N-body simulations. We take the particle data at redshift $z=1$, $z=0.5$, and $z=0$ from TNG300-3-Dark, a low-resolution dark matter-only run of the TNG300 series, and feed the particles to LDL models. In the next section we compare the performance of these two hybrid simulations against the target high-resolution hydrodynamical simulation.

We summarize the numerical parameters of these simulations in Table 1. We also list TNG300-3, the low-resolution hydrodynamic run of TNG300. TNG300-3 has the resolution of our hybrid simulations and is a natural reference to compare the performance of our models with. Note that the mass resolution, force/mesh resolution, and time resolution of our hybrid simulations are significantly lower than those of the target simulation, and the N-body simulation and deep-learning networks are also much cheaper to run compared to simulating hydrodynamics. As a result, the FastPM-based and N-body-based hybrid simulations are 7 and 4 orders of magnitudes cheaper than the target simulation, respectively. When comparing to TNG300-3, our hybrid simulations are still 4 and 1 orders of magnitude cheaper, respectively, and we show that by being trained on the high-resolution TNG300-1 our simulations are superior to TNG300-3 and comparable to TNG300-1.

Results

We show in Fig. 1 the visualization of slices of the input linear density field and the output dark matter of our FastPM-based hybrid simulation, as well as the target fields in hydrodynamical simulation. Visual agreement between the two is very good. The results are shown for the dark matter density, stellar mass density, electron momentum density $n_e v_z$, where n_e is electron density and v_z radial velocity; electron pressure $n_e T$, where T is the gas temperature; and X-ray emission proportional to $n_e^2 T^{0.5}$.

Power Spectrum. We measure the summary statistics of these fields and compare them quantitatively. We first compare the power spectrum, the most widely used summary statistic in cosmology. We define the transfer function as

$$T(k) = \sqrt{\frac{P_{\mathrm{predict}}(k)}{P_{\mathrm{target}}(k)}} \quad [6]$$

and the cross-correlation coefficient as

Table 1. The numerical parameters of LDL hybrid simulations, low-resolution TNG300-3, and the target TNG300-1 hydrodynamical simulations

	FastPM + LDL	TNG300-3-Dark + LDL	TNG300-3	TNG300-1
N_{particle}	625^3	625^3	$N_{\mathrm{DM}}=625^3$ $N_{\mathrm{gas}}=625^3$	$N_{\mathrm{DM}}=2{,}500^3$ $N_{\mathrm{gas}}=2{,}500^3$
Force/mesh resolution (h^{-1}ckpc)	164 (FastPM) 328 (LDL)	4.0 (TNG-Dark) 328 (LDL)	$\epsilon_{\mathrm{DM},*}=4.0$ $\epsilon_{\mathrm{gas}}=1.0$	$\epsilon_{\mathrm{DM},*}=1.0$ $\epsilon_{\mathrm{gas}}=0.25$
No. of time steps/ layers	$N_{\mathrm{FastPM}}=10$ $N_{\mathrm{LDL},*}=4$	$N_{\mathrm{TNG}}=9{,}201$ $N_{\mathrm{LDL},*}=3$	209, 161	6, 203, 062
CPU time	$T_{\mathrm{IC}}=2.3$ $T_{\mathrm{FastPM}}=5.1$ h $T_{\mathrm{LDL},*}=0.4$ h	$T_{\mathrm{TNG}}=5.9$ kh $T_{\mathrm{LDL},*}=0.3$ h	0.05 Mh	34.9 Mh

The LDL parameters for generating stellar mass are shown. The architecture for other observables can be found in Table 2. The total CPU time for LDL is 7.8 h, compared to 5×10^4 for the full hydro-TNG300-3. Despite this the LDL generally outperforms the full hydro at the same resolution. In this paper we are primarily concerned with a proof of principle and both FastPM and LDL are run with Python. We expect the CPU time to be further reduced if running them with C.

$$r(k) = \frac{P_{\rm predict,target}(k)}{\sqrt{P_{\rm predict}(k) P_{\rm target}(k)}}, \quad [7]$$

where $P_{\rm predict,target}(k)$ is the cross-power spectrum between the predicted field and the target field. We show the 3D or 2D power spectrum, transfer function, and cross-correlation coefficient of the stellar mass overdensity δ_*, electron momentum $n_e v_z$, electron pressure $n_e T$, and X-ray intensity $n_e^2 T^{0.5}$ in Figs. 2–5, respectively. On the large scale and the intermediate scale our hybrid simulations in general match well with the target fields (except for the case of X-ray, where FastPM-based hybrid simulations fail to predict correct large-scale power at redshifts 0.5 and 1), while TNG300-3 agreement is generally worse, especially for the stellar mass. The large bias of TNG300-3 stellar mass might be partially due to the fact that the low-resolution TNG300-3 cannot resolve the stars in small halos. In contrast, by training on high-resolution hydrosimulations TNG300-1, our low-resolution hybrid simulations are able to model those small galaxies better than the full hydrosimulation at the same resolution.

On the small scales all of the predicted fields show some deviations from the targets. We discuss possible reasons for these in the next section. We also see that the full-N-body–based hybrid simulation normally predicts larger small-scale power than the FastPM-based simulation. This is likely due to the fact that the 10-layer FastPM cannot fully model the small halos and halo internal structures, and its simulated dark matter distribution is less clustered on small scale compared to full N-body simulations, making its predicted baryon fields less clustered. Overall, the predicted power spectrum from the N-body–based hybrid simulation is better, although it can predict too much small-scale power (e.g., the kSZ signal at redshift 1). This inaccuracy of small-scale matter distribution of FastPM could also explain the inconsistency of its predicted large-scale power of X-ray at redshifts 0.5 and 1. Since the X-ray signal is proportional to n_e^2, its large-scale power is correlated to the small-scale fluctuations of the n_e field. This modeling task is not easy for FastPM, but N-body–based hybrid simulation is able to model it quite well (Fig. 5).

The cross-correlation coefficients are also shown in Figs. 2–5. We observe that the hybrid simulations are significantly better than those of TNG300-3, with the N-body–based hybrid simulation a bit higher than the FastPM-based simulation. Note that in principle the cross-correlation coefficient, which quantifies the agreement of phases of Fourier modes, is a more important statistic than the transfer function, because the transfer function can always be corrected to unity by multiplying the predicted fields with the reciprocal of the transfer function. This again suggests that the baryon maps of our models are closer to the ground truth than full hydrodynamical simulations at the same resolution.

Cross-Correlations between Different Tracers. Probes of the large-scale structure, such as weak lensing, galaxy survey, and clusters, are strongly correlated because they are all determined by the same underlying matter distribution. There is additional information in the cross-correlations between these probes which cannot be obtained by analyzing each observable independently. The cross-correlation also has the advantage that the noise does not add to it. Our hybrid simulation is able to generate various observables simultaneously with a low computational cost, so it is potentially promising for cross-correlation analysis. Here we

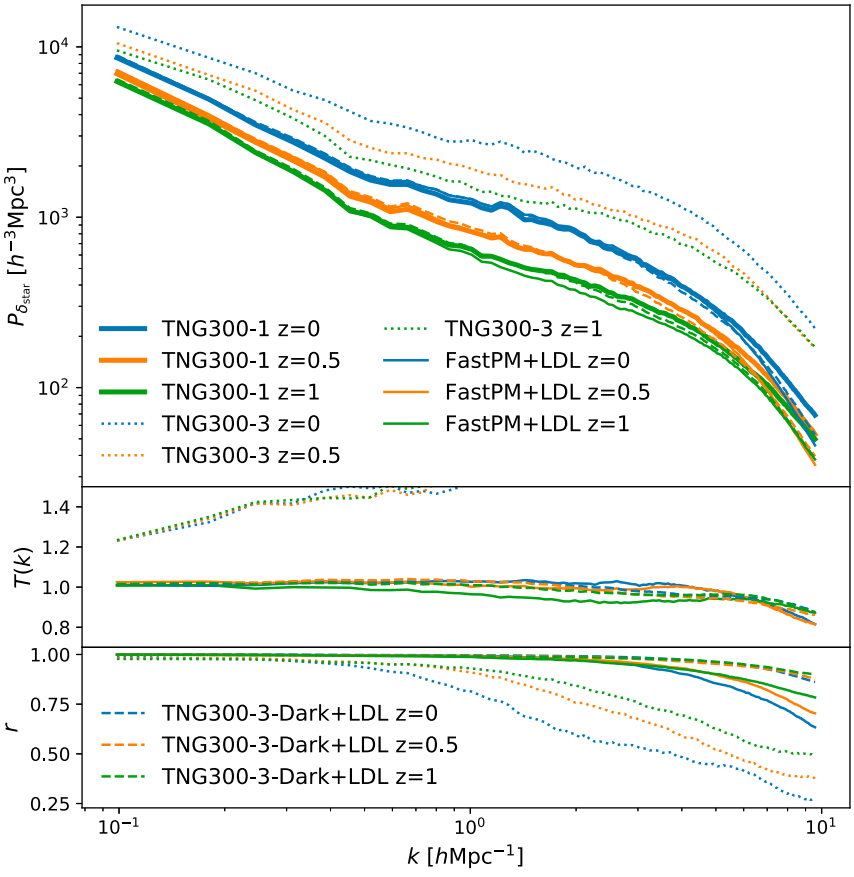

Fig. 2. Comparison of the test set 3D power spectrum (*Top*), transfer function (*Middle*), and cross-correlation coefficient (*Bottom*) of the stellar mass overdensity. We compare LDL hybrid simulations, TNG300-3, and the target TNG300-1 hydrodynamical simulation, at redshifts 0, 0.05, and 1.

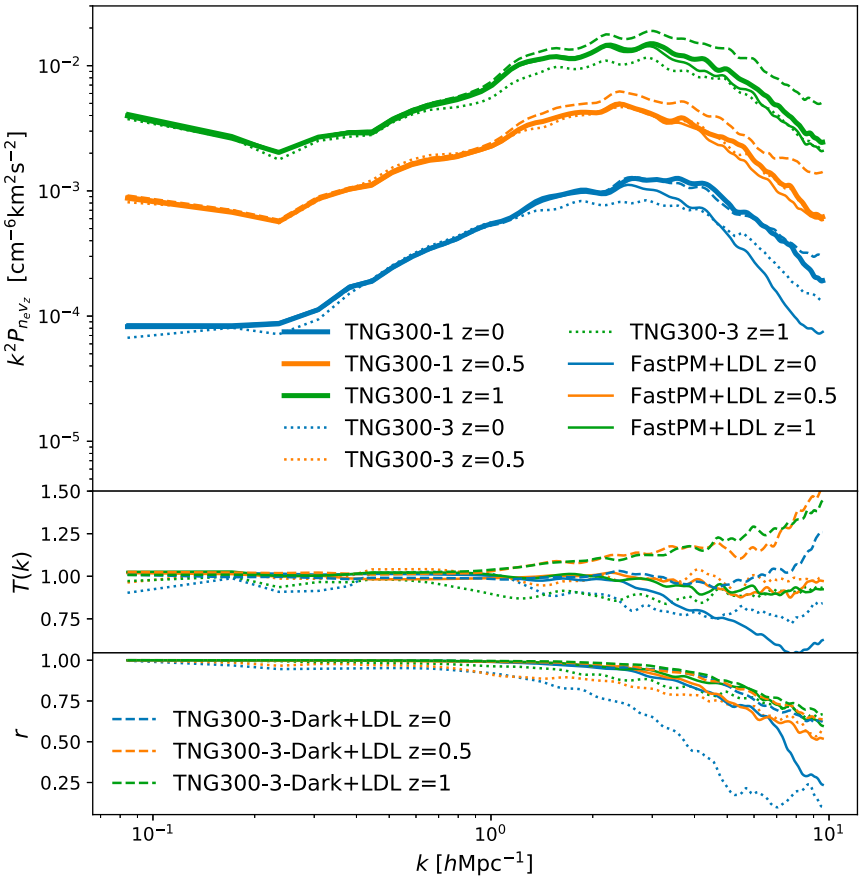

Fig. 3. Comparison of the test set 2D power spectrum (*Top*), transfer function (*Middle*), and cross-correlation coefficient (*Bottom*) of the electron momentum density $n_e v_z$ (proportional to kSZ signal) between the LDL hybrid simulations, TNG300-3, and the target TNG300-1 hydrodynamical simulation. The 90.2 h^{-1}Mpc subbox of the test set is projected along the z axis for the calculation of the 2D power spectrum.

investigate the predicted cross-correlations between weak lensing convergence, mass weighted galaxies, tSZ, and X-ray, as well as the cross-correlation between the galaxy momentum and kSZ signal. We show the ratio of the predicted cross-power spectrum and the TNG300-1 in Fig. 6. Similar to the autopower spectrum analysis, our predicted cross-power spectrum is in general consistent with the target simulation on a large scale (except for the cases involving X-ray predicted with FastPM, and we discuss possible reasons in the previous section), while TNG300-3 does not agree so well. On small scales FastPM-based hybrid simulation tends to underestimate the power, while TNG300-3 tends to overestimate the power. One can compare the second panel of Fig. 6 (cross-power spectrum between the matter and tSZ) with figure 2 of ref. 18, where GAN and VAE are used to predict the gas pressure from N-body simulations. We observe that the deviation of full-N-body–based hybrid simulation is comparable to the deviations of GAN and VAE. We note that for the standard deep-learning architectures employed by GAN or VAE the number of parameters being fitted is very large, in contrast to our approach.

Discussion

We propose a LDL model for learning the effective physical laws from the outputs of either simulations or real data. Specifically, in this paper we focus on learning the physics that control baryon hydrodynamics in the cosmological simulations. We build hybrid simulations by combining an N-body/quasi–N-body gravity solver with LDL models. We show that both the FastPM-based and N-body–based hybrid simulations are able to generate maps of stellar mass, kSZ, tSZ, and X-ray of various redshifts from the linear density field, and their computational costs are 7 and 4 orders of magnitude lower than that of the target high-resolution hydrodynamical simulation. We perform the autopower spectrum analysis and the cross-correlation analysis among these fields, and we show that they generally outperform the hydrodynamical simulation at the same resolution.

The LDL model is motivated by the desire to provide an effective description of the underlying physics. Such a description must obey all of the symmetries of the problem, and rotation and translation invariance are the two key symmetries, but other symmetries of the problem such as mass conservation may also appear. In this paper we argue that implementing these symmetries creates a generative model that is learning an effective description of the physical laws as opposed to learning the data distribution. This is because the symmetries are the only constraints on the generative model that must be implemented explicitly; everything else can be learned from the data. Here we propose that the learning of the generative model can be implemented by composing layers of displacements acting on the effective particles describing the physical properties of a system such as a fluid, moving the particles following the Lagrangian approach. The displacement of the particles can be understood as a result of the underlying physical processes, with particle transport a consequence of processes such as gas cooling and heating, feedback, and turbulence, etc. The output layer is a nonlinear transformation with thresholding on the particle density field, which models physics processes such as star formation.

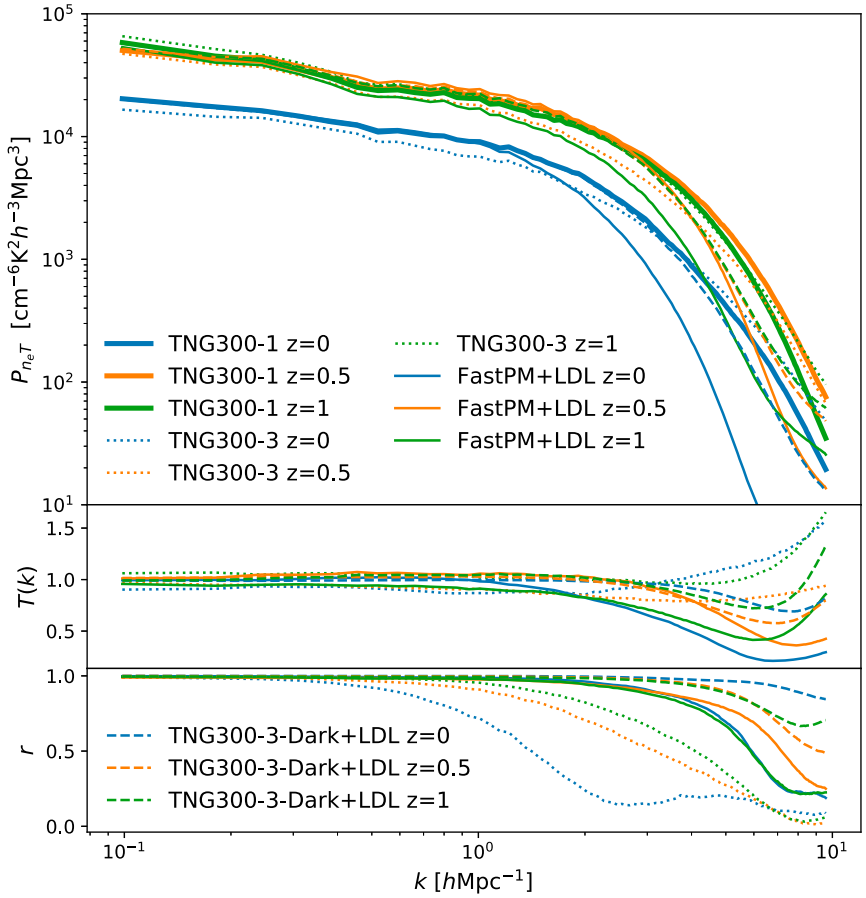

Fig. 4. Comparison of the test set 3D power spectrum (*Top*), transfer function (*Middle*), and cross-correlation coefficient (*Bottom*) of the electron pressure n_eT (proportional to tSZ signal) between the LDL hybrid simulations, TNG300-3, and the target TNG300-1 hydrodynamical simulation.

Translational and rotational symmetry of the system puts strong constraints on the model and therefore the Green's operator can be written as a function in Fourier space that depends only on the amplitude of k. This allows us to use very few parameters to model the complex processes and produce maps of observables. Thus even though we want to describe systems of extremely high dimensionality (10^8 or more), the underlying effective physics description requires a handful of parameters only.

The small number of free parameters also makes the model stable and easy to train. An important advantage is that we can use the small number of parameters as an effective physics description of a complicated microphysics model, similar to the free parameters that arise from renormalization in the effective field theory descriptions of microphysics. This suggests that our LDL approach can replace other effective descriptions used to model the process of star formation. In cosmology such simplified models are often based on first identifying the dark matter halos in a dark matter simulation only, followed by some effective description of how to populate these halos with stars. Compared to such semianalytical approaches which often rely on nondifferentiable models, our approach is explicitly differentiable, such that we can use backpropagation to derive a gradient of the final observables with respect to the initial density field. This can be easily embedded into the forward modeling framework to reconstruct the initial conditions from the observations (37).

Our current implementation generally outperforms the full hydrosimulation at the same resolution, but does not match perfectly the higher-resolution hydrosimulation. LDL deviates from the full simulation results mostly on small scales. This is expected, since the factor of 64 lower mass resolution means there is some information in the full simulation that cannot be recovered. Specifically, we use a low-resolution mesh for calculating the displacements in the LDL model (cell size $0.328h^{-1}\mathrm{Mpc}$) (Table 1). The low-resolution mesh limits the ability of LDL to model the small-scale baryon distribution. Moreover, to ensure the correct large-scale distribution, we apply a smoothing operator (Eq. **9**) to the fields before calculating the loss function, which down-weights the small-scale contribution to the loss function.

LDL trains on hydrodynamic simulations and is not meant to replace but to complement them: For example, it can interpolate a coarse grid and scale them to larger volumes and higher resolutions. In contrast, LDL has the potential to eliminate the need for the semianalytic methods, which are the current standard paradigm in the large-scale structure. These methods run N-body simulations first and then populate their dark matter halos using a semianalytic prescription for the observable. LDL can not only achieve results that are on par with the full hydro at the same resolution, which is superior to these semianalytic approaches; it also achieves them with of order 10 time steps, in addition to up to 6 LDL layers, in contrast to 10^3 in an N-body simulation. We expect this will lead both to development of realistic simulations that cover the full volume of the cosmological large-scale structure (LSS) surveys and to analysis of these LSS surveys with LDL effective parameters as the nuisance parameters describing the astrophysics of the galaxy formation.

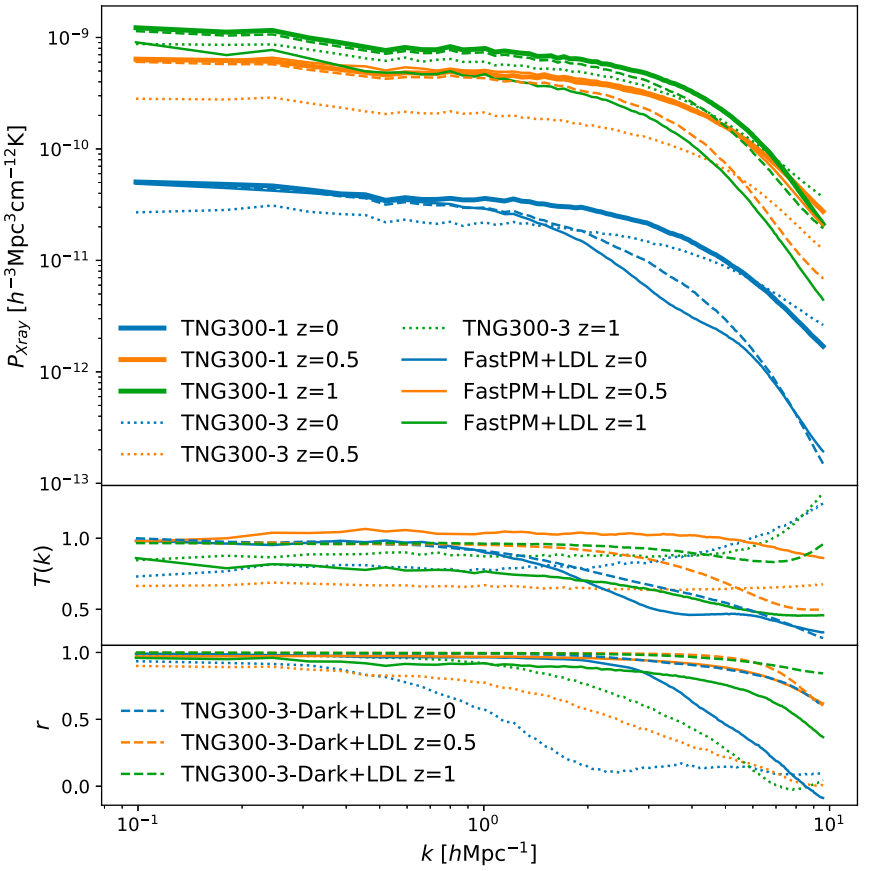

Fig. 5. Comparison of the test set 3D power spectrum (*Top*), transfer function (*Middle*), and cross-correlation coefficient (*Bottom*) of the gas property $n_e^2 T^{0.5}$ (proportional to X-ray emissivity) between the LDL hybrid simulations, TNG300-3, and the target TNG300-1 hydrodynamical simulation.

Materials and Methods

Dataset. IllustrisTNG is a suite of cosmological magnetohydrodynamical simulations of galaxy formation and evolution (26–30). It consists of three runs of different volumes and resolutions: TNG50, TNG100, and TNG300 with side lengths of $35h^{-1}$Mpc ≈ 50Mpc, $75h^{-1}$Mpc ≈ 100Mpc, and $205h^{-1}$Mpc ≈ 300Mpc, respectively. IllustrisTNG follows the evolution of the dark

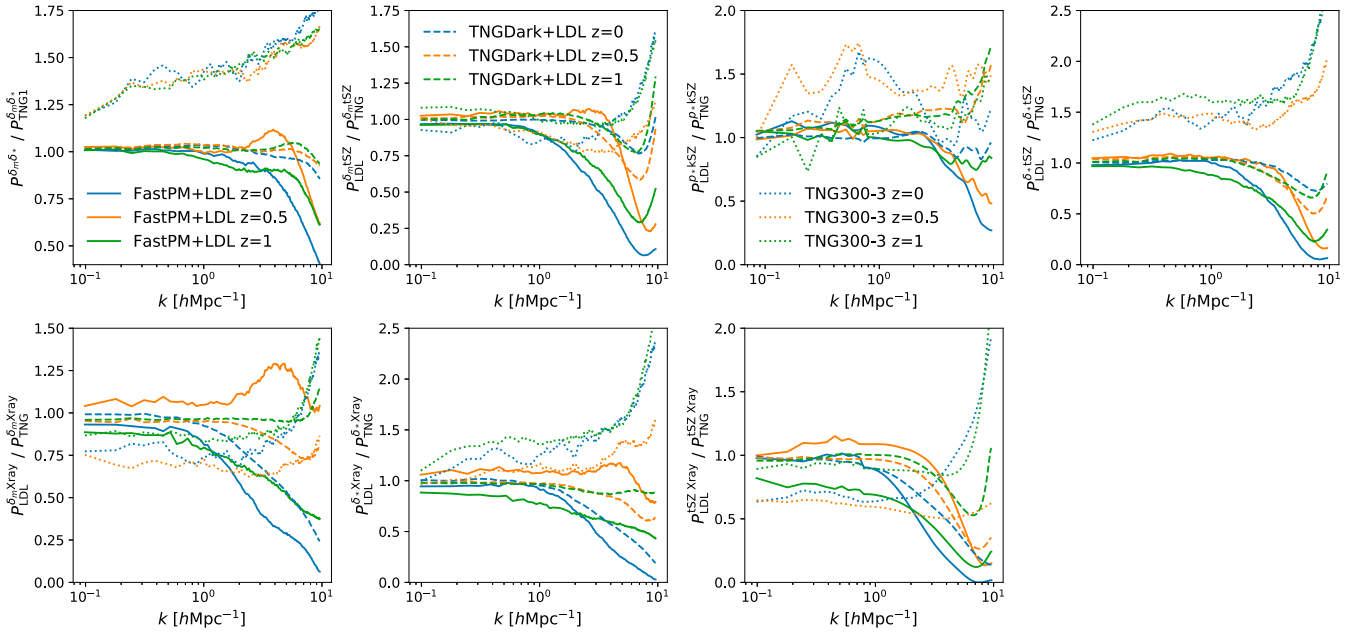

Fig. 6. The ratio of the test set cross-power spectrum of different observables between the LDL hybrid simulations and the target TNG300-1 hydrodynamical simulation. *Top* row shows the cross-power spectrum of matter and stellar mass (first panel), matter and tSZ signal (second panel), 2D stellar momentum density and kSZ signal (third panel), and stellar mass and tSZ signal (fourth panel). *Bottom* row shows the cross-power spectrum of matter and X-ray (first panel), stellar mass and X-ray (second panel), and tSZ and X-ray (third panel).

matter, gas, stars, and supermassive black holes, with a full set of physical models including star formation and evolution, supernova feedback with galactic wind, primordial and metal-line gas cooling, chemical enrichment, black hole formation, growth, and multimode feedback. The IllustrisTNG series evolves over a redshift range $z = 127$ to the present $z = 0$ in a ΛCDM cosmology, with parameters $\Omega_m = 0.3089$, $\Omega_b = 0.0486$, $\Omega_\Lambda = 0.6911$, $H_0 = 67.74$ km·s^{-1}·Mpc^{-1}, $\sigma_8 = 0.8159$, and $n_s = 0.9667$.

In this paper we train our models against TNG300-1, the highest resolution of the TNG300 run. TNG300-1 evolves $2{,}500^3$ dark matter particles and an initial number of $2{,}500^3$ gas cells, with a comoving force resolution $\epsilon_{\mathrm{DM,stars}} = 1.0h^{-1}$kpc, $\epsilon_{\mathrm{gas,min}} = 0.25h^{-1}$kpc, and $\epsilon_{\mathrm{BH,max}} = 5.84h^{-1}$kpc. The dark matter mass resolution is $4.0 \times 10^7 h^{-1} M_\odot$, and the target baryon mass resolution is $7.6 \times 10^6 h^{-1} M_\odot$ (Table 1).

We also compare the model performance with TNG300-3, the hydro run with the same resolution as our hybrid simulations. The mass resolution and force resolution of TNG300-3 are 64 and 4 times lower than that of TNG300-1, respectively.

Details of the Hybrid Simulation. The 10-step FastPM is run in a $205h^{-1}$Mpc periodic box, but with only $N = 625^3$ particles and force resolution $B = 2$. We generate the initial condition at redshift $z = 9$ using second-order Lagrangian perturbation theory (2LPT), with the same random seed and linear power spectrum as IllustrisTNG. The linear density map is generated with a $N = 1{,}250^3$ mesh to improve the accuracy on a small scale (33). The box is then evolved to redshift 0 with 10 time steps that are linearly separated in scale factor a. Three snapshots are produced at redshifts $z = 0$, 0.5, and 1, which are passed to LDL for generating maps of baryonic observables at these redshifts. Note that our mass, force, and time resolutions are 64, 164, and 620,000 times lower than those of the target simulation TNG300-1, respectively.

Instead of running 10-step FastPM, we also tried using the particle data from the full N-body simulation TNG300-3-Dark. TNG300-3-Dark is the dark matter-only run of the low-resolution TNG300-3. It includes $N = 625^3$ dark matter particles (same as our FastPM setup), but the force and time resolutions are significantly higher. A detailed comparison between FastPM, TNG300-3-Dark, and TNG300-1 can be found in Table 1.

The details of the LDL model are described in the main text. We use a $N = 625^3$ mesh for calculating the displacement and generating the hydro maps. The architecture of the model is shown in Table 2. Specifically, for FastPM input, we first add a Lagrangian displacement layer and the output is matched to the density field of the full N-body simulation TNG300-3-Dark. This layer is intended to improve the small-scale structure of FastPM and is shared by all hydro outputs (we do not add this layer for TNG300-3-Dark input). Then for different observables, we train different displacement layers and output layer: 1) For stellar mass, we add two displacement layers to mimic gas cooling and collapse and one output layer to model star formation. 2) For kSZ signal, we use one displacement layer and one output layer to model the electron number density field. We assume that the velocities of gas trace dark matter, so the velocity field can be directly estimated from the dark matter particles: $v(x) = \frac{p(x)}{\rho(x)}$, where $p(x)$ is the momentum density field and $\rho(x)$ is the matter density field. The kSZ map is obtained by multiplying the electron density field and the velocity field. 3) For the tSZ signal map, we generate the electron number density field with one displacement layer and one output layer and generate the gas temperature map with two displacement layers and one output layer. Then the two fields are multiplied to produce the tSZ signal. 4) The modeling of X-ray is similar to that of tSZ, except that now we use two displacement layers to model the electron density.

Model Training and Loss Function. As described above, the output of the LDL model is a $N = 625^3$ mesh. We retain 77.7% of the pixels for training, 13.8% for validation, and 8.5% for test. Similar to ref. 17, we split between training, validation, and test sets following a "global" cut. The test set forms a subbox of $90.2h^{-1}$Mpc per side, and the validation set is a $90.2 \times 114.8 \times 114.8$ h^{-1}Mpc subbox. The rest of the $205h^{-1}$Mpc box is used for training.

Table 2. The LDL architecture for predicting different baryon observables

	Stellar mass	kSZ		tSZ		X-ray	
		n_e	v_z	n_e	T	n_e	T
Displacement layer (Eq. **1**)	2	1	0	1	2	2	2
Output layer (Eq. **5**)	1	1	0	1	1	1	1
Total no. of layers	3 (4)	2 (3)		5 (6)		6 (7)	
Total no. of free parameters	13 (18)	8 (13)		21 (26)		26 (31)	

For FastPM-based hybrid simulation, we add one more displacement layer to improve the small-scale dark matter distribution. The corresponding N_{layer} and $N_{\mathrm{parameter}}$ are shown in parentheses.

For stellar mass and the electron number density field in the kSZ map, we define the loss function as

$$\mathcal{L} = \sum_{i=1}^{N} \|\hat{\mathbf{O}}_{\mathbf{s}} F_{\mathrm{LDL}}(x_i) - \hat{\mathbf{O}}_{\mathbf{s}} F_{\mathrm{TNG}}(x_i)\|, \quad [8]$$

where $\|$ is L_1 norm, i labels the mesh cell, $F_{\mathrm{LDL}}(x)$ is the generated map from LDL, $F_{\mathrm{TNG}}(x)$ is the true hydro map from IllustrisTNG, and $\hat{\mathbf{O}}_{\mathbf{s}}$ is a smoothing operator defined in Fourier space:

$$\hat{\mathbf{O}}_{\mathbf{s}} = 1 + \left(\frac{k}{1h\mathrm{Mpc}^{-1}}\right)^{-n}. \quad [9]$$

Here n is a hyperparameter that determines the relative weight between the large-scale modes and the small-scale modes. Without the $\hat{\mathbf{O}}_{\mathbf{s}}$ operator, the model focuses on the small-scale distribution and results in a biased large-scale power due to the small number of large-scale modes relative to small-scale modes. We apply the $\hat{\mathbf{O}}_{\mathbf{s}}$ operator to put more weight on the large-scale distribution. For most of the baryon maps we fix $n = 1$, except for the X-ray map we optimize the hyperparameter n.

For the tSZ map, we use a different loss function to improve the performance. We first train the electron density map with the loss function

$$\mathcal{L}_{n_e}^{\mathrm{tSZ}} = \sum_{i=1}^{N} \|\hat{\mathbf{O}}_{\mathbf{s}}[n_{e_{\mathrm{LDL}}}(x_i) T_{\mathrm{TNG}}(x_i)] - \hat{\mathbf{O}}_{\mathbf{s}}[n_{e_{\mathrm{TNG}}}(x_i) T_{\mathrm{TNG}}(x_i)]\|, \quad [10]$$

where $n_{e_{\mathrm{LDL}}}(x)$ is the learned electron number density map, $n_{e_{\mathrm{TNG}}}(x)$ is the true electron number density map, and T_{TNG} is the true temperature map. This means we multiply the electron number density field by the temperature field before calculating the loss function. This procedure puts more weight on the large clusters and improves the quality of the generated tSZ maps. Note that this electron density field is different from the electron density field for predicting the kSZ signal. Similarly, after we obtain the learned electron number density field $n_{e_{\mathrm{LDL}}}(x)$, we train the temperature map with the following the loss function:

$$\mathcal{L}_{T}^{\mathrm{tSZ}} = \sum_{i=1}^{N} \|\hat{\mathbf{O}}_{\mathbf{s}}[n_{e_{\mathrm{LDL}}}(x_i) T_{\mathrm{LDL}}(x_i)] - \hat{\mathbf{O}}_{\mathbf{s}}[n_{e_{\mathrm{TNG}}}(x_i) T_{\mathrm{TNG}}(x_i)]\|. \quad [11]$$

Here $n_{e_{\mathrm{LDL}}}(x)$ is the electron density field we just learned and is fixed, and $T_{\mathrm{LDL}}(x)$ is the target temperature field that we are trying to optimize.

For the X-ray map, similar to the tSZ signal, we train the electron density and gas temperature maps successively with the following loss functions:

$$\mathcal{L}_{n_e}^{\mathrm{X}} = \sum_{i=1}^{N} \|\hat{\mathbf{O}}_{\mathbf{s}}[n_{e_{\mathrm{LDL}}}^2(x_i) T_{\mathrm{TNG}}^{0.5}(x_i)] - \hat{\mathbf{O}}_{\mathbf{s}}[n_{e_{\mathrm{TNG}}}^2(x_i) T_{\mathrm{TNG}}^{0.5}(x_i)]\|, \quad [12]$$

$$\mathcal{L}_{T}^{\mathrm{X}} = \sum_{i=1}^{N} \|\hat{\mathbf{O}}_{\mathbf{s}}[n_{e_{\mathrm{LDL}}}^2(x_i) T_{\mathrm{LDL}}^{0.5}(x_i)] - \hat{\mathbf{O}}_{\mathbf{s}}[n_{e_{\mathrm{TNG}}}^2(x_i) T_{\mathrm{TNG}}^{0.5}(x_i)]\|. \quad [13]$$

Again, the electron number density field and gas temperature field for X-ray are different from the fields used for generating kSZ and tSZ.

Because the number of free parameters is relatively small, in this work we use the L-BFGS-B algorithm (38) for optimizing the model parameters. The training time varies with the target. A typical training (e.g., stellar mass) takes a couple of hours on four Cori nodes of National Energy Research Scientific Computing Center (NERSC), which corresponds to a few hundred central processing unit (CPU) hours.

Data Availability. The source code has been deposited in Github (https://github.com/biweidai/LDL). The data of TNG simulation is available at https://www.tng-project.org/data/ (39).

ACKNOWLEDGMENTS. We thank Dylan Nelson and the IllustrisTNG team for kindly providing the linear power spectrum, random seed, and the numerical parameters of the IllustrisTNG simulations. We thank Yu Feng for helpful discussions. This material is based on work supported by the

NSF under Grants 1814370 and NSF 1839217 and by NASA under Grant 80NSSC18K1274. Most of the computations were performed at the NERSC computing facilities Cori, billed under the cosmosim and m3058 repository. NERSC is a US Department of Energy Office of Science User Facility operated under Contract DE-AC02-05CH11231. The power spectrum analysis in this work is performed using the open-source toolkit nbodykit.

1. D. J. Eisenstein *et al.*, SDSS-III: Massive spectroscopic surveys of the distant universe, the milky way, and extra-solar planetary systems. *Astron. J.* **142**, 72 (2011).
2. Z. Ivezic *et al.*, LSST: From science drivers to reference design and anticipated data products. *Bull. Am. Astron. Soc.* **41**, 366 (2009).
3. D. Spergel *et al.*, Wide-field infrarred survey telescope-astrophysics focused telescope assets WFIRST-AFTA 2015 report. arXiv [Preprint] (2015). https://arxiv.org/abs/1503.03757 (Accessed 6 April 2021).
4. A. Aghamousa *et al.*, The DESI experiment part I: Science, targeting, and survey design. arXiv [Preprint] (2016). https://arxiv.org/abs/1611.00036 (Accessed 6 April 2021).
5. L. Amendola *et al.*, Cosmology and fundamental physics with the Euclid satellite. *Living Rev. Relat.* **21**, 2 (2018).
6. V. Springel *et al.*, Simulations of the formation, evolution and clustering of galaxies and quasars. *Nature* **435**, 629–636 (2005).
7. J. DeRose *et al.*, The Aemulus project. I. Numerical simulations for precision cosmology. *Astrophys. J.* **875**, 69 (2019).
8. A. A. Berlind, D. H. Weinberg, The halo occupation distribution: Toward an empirical determination of the relation between galaxies and mass. *Astrophys. J.* **575**, 587 (2002).
9. P. Behroozi, R. H. Wechsler, A. P. Hearin, C. Conroy, Universemachine: The correlation between galaxy growth and dark matter halo assembly from z = 0-10. *Mon. Not. R. Astron. Soc.* **488**, 3143–3194 (2019).
10. I. Goodfellow *et al.*, "Generative adversarial nets" in *Advances in Neural Information Processing Systems*, Z. Ghahramani, M. Welling, C. Cortes, N. Lawrence, K. Q. Weinberger, Eds. (MIT Press, 2014), pp. 2672–2680.
11. D. P. Kingma, M. Welling, Auto-encoding variational Bayes. arXiv [Preprint] (2013). https://arxiv.org/abs/1312.6114 (Accessed 4 April 2021).
12. D. J. Rezende, S. Mohamed, D. Wierstra, Stochastic backpropagation and approximate inference in deep generative models. arXiv [Preprint] (2014). https://arxiv.org/abs/1401.4082 (Accessed 6 April 2021).
13. C. Modi, Y. Feng, U. Seljak, Cosmological reconstruction from galaxy light: Neural network based light-matter connection. *J. Cosmol. Astropart. Phys.* **2018**, 028 (2018).
14. P. Berger, G. Stein, A volumetric deep convolutional neural network for simulation of mock dark matter halo catalogues. *Mon. Not. R. Astron. Soc.* **482**, 2861–2871 (2019).
15. D. K. Ramanah, T. Charnock, G. Lavaux, Painting halos from cosmic density fields of dark matter with physically motivated neural networks. *Phys. Rev. D* **100**, 043515 (2019).
16. M. Bernardini, L. Mayer, D. Reed, R. Feldmann, Predicting dark matter halo formation in n-body simulations with deep regression networks. *Mon. Not. R. Astron. Soc.* **496**, 5116–5125 (2020).
17. X. Zhang *et al.*, From dark matter to galaxies with convolutional networks. arXiv [Preprint] (2019). https://arxiv.org/abs/1902.05965 (Accessed 6 April 2021).
18. T. Tröster, C. Ferguson, J. Harnois-Déraps, I. G. McCarthy, Painting with baryons: Augmenting n-body simulations with gas using deep generative models. *Mon. Not. R. Astron. Soc. Lett.* **487**, L24–L29 (2019).
19. F. List, I. Bhat, G. F. Lewis, A black box for dark sector physics: Predicting dark matter annihilation feedback with conditional GANs. *Mon. Not. R. Astron. Soc.* **490**, 3134–3143 (2019).
20. E. Giusarma *et al.*, Learning neutrino effects in cosmology with convolutional neural networks. arXiv [Preprint] (2019). https://arxiv.org/abs/1910.04255 (Accessed 6 April 2021).
21. D. K. Ramanah, T. Charnock, F. Villaescusa-Navarro, B. D. Wandelt, Super-resolution emulator of cosmological simulations using deep physical models. *Mon. Not. R. Astron. Soc.* **495**, 4227–4236 (2020).
22. Y. Li *et al.*, AI-assisted super-resolution cosmological simulations. arXiv [Preprint] (2020). https://arxiv.org/abs/2010.06608 (Accessed 6 April 2021).
23. S. Tassev, M. Zaldarriaga, D. J. Eisenstein, Solving large scale structure in ten easy steps with Cola. *J. Cosmol. Astropart. Phys.* **2013**, 036 (2013).
24. Y. Feng, M.-Y. Chu, U. Seljak, P. McDonald, FastPM: A new scheme for fast simulations of dark matter and haloes. *Mon. Not. R. Astron. Soc.* **463**, 2273–2286 (2016).
25. S. He *et al.*, Learning to predict the cosmological structure formation. *Proc. Natl. Acad. Sci. U.S.A.* **116**, 13825–13832 (2019).
26. A. Pillepich *et al.*, First results from the IllustrisTNG simulations: The stellar mass content of groups and clusters of galaxies. *Mon. Not. R. Astron. Soc.* **475**, 648–675 (2018).
27. J. P. Naiman *et al.*, First results from the IllustrisTNG simulations: A tale of two elements–chemical evolution of magnesium and europium. *Mon. Not. R. Astron. Soc.* **477**, 1206–1224 (2018).
28. F. Marinacci *et al.*, First results from the IllustrisTNG simulations: Radio haloes and magnetic fields. *Mon. Not. R. Astron. Soc.* **480**, 5113–5139 (2018).
29. V. Springel *et al.*, First results from the IllustrisTNG simulations: Matter and galaxy clustering. *Mon. Not. R. Astron. Soc.* **475**, 676–698 (2018).
30. D. Nelson *et al.*, First results from the IllustrisTNG simulations: The galaxy colour bimodality. *Mon. Not. R. Astron. Soc.* **475**, 624–647 (2018).
31. J. J. M. Carrasco, M. P. Hertzberg, L. Senatore, The effective field theory of cosmological large scale structures. *J. High Energy Phys.* **2012**, 82 (2012).
32. B. Dai, Y. Feng, U. Seljak, A gradient based method for modeling baryons and matter in halos of fast simulations. *J. Cosmol. Astropart. Phys.* **2018**, 009 (2018).
33. B. Dai, Y. Feng, U. Seljak, S. Singh, High mass and halo resolution from fast low resolution simulations. *J. Cosmol. Astropart. Phys.* **2020**, 002 (2020).
34. D. H. Rudd, A. R. Zentner, A. V. Kravtsov, Effects of baryons and dissipation on the matter power spectrum. *Astrophys. J.* **672**, 19 (2008).
35. M. P. van Daalen, J. Schaye, C. M. Booth, C. D. Vecchia, The effects of galaxy formation on the matter power spectrum: A challenge for precision cosmology. *Mon. Not. R. Astron. Soc.* **415**, 3649–3665 (2011).
36. H.-J. Huang, T. Eifler, R. Mandelbaum, D. Scott, Modelling baryonic physics in future weak lensing surveys. *Mon. Not. R. Astron. Soc.* **488**, 1652–1678 (2019).
37. U. Seljak, G. Aslanyan, F. Yu, C. Modi, Towards optimal extraction of cosmological information from nonlinear data. *J. Cosmol. Astropart. Phys.* **2017**, 009 (2017).
38. R. H. Byrd, P. Lu, J. Nocedal, C. Zhu, A limited memory algorithm for bound constrained optimization. *SIAM J. Sci. Comput.* **16**, 1190–1208 (1995).
39. D. Nelson *et al.*, The IllustrisTNG simulations: Public data release. *Comput. Astrophys. Cosmol.* **6**, 1–29 (2019).